The effect of pressure on the elastic properties and seismic anisotropy of diopside and jadeite from atomic scale simulation

Andrew M. Walker [a,*]

[a] *School of Earth Sciences, University of Bristol, Wills Memorial Building, Queens Road, Bristol, BS8 1RJ, UK*

Abstract

Preprint submitted to Elsevier Science *6 October 2011*

The full elastic constants tensors of diopside ($CaMgSi_2O_6$) and jadeite ($NaAlSi_2O_6$) have been calculated using a planewave and pseudopotentials based implementation of density functional theory within the generalised gradient approximation at pressures between 0 and 20 GPa. Both minerals stiffen over this pressure range with the isotropic average bulk moduli increasing by ∼50 % and the shear moduli by ∼20 %. However, in detail the behaviour of the individual elastic constants varies and this drives changes in the anisotropy. Overall, and in contrast to predictions based on the extrapolation of calculations based on inter-atomic potential models, the elastic anisotropy of diopside decreases with increasing pressure. The elastic anisotropy of jadeite increases slightly at low pressure, exhibits a maximum at around 10 GPa and then begins to slowly decrease. Despite the small changes in the total and maximum anisotropy, the shear-wave anisotropy for certain propagation directions vary dramatically with pressure. For example, the anisotropy experienced by a shear-wave propagating in the [010] direction in diopside doubles between 5 and 15 GPa.

Key words: Elasticity, Clinopyroxene, Shear-wave splitting, Density functional theory

1 Introduction

Many of the strongest constraints on the composition and behaviour of the Earth's interior come from seismic observations. When combined with a database of the elastic properties and densities of Earth materials under the relevant conditions of high pressure and temperature, the travel times of seismic

* phone: +44 (0)117 9545245, fax: +44 (0)117 9253385
Email address: andrew.walker@bristol.ac.uk (Andrew M. Walker).

waves provide insight on the variation of temperature and composition of the deep interior. Furthermore, knowledge of the full elastic constants tensor can be used to interpret the different travel times of perpendicularly polarised shear waves in terms of a crystal preferred orientation caused by convectively driven deformation. To make best use of our growing seismic data sets, it is necessary to know how the elastic constants, C_{ij} (throughout this article contracted Voigt notation is used to express the fourth-order elastic stiffness tensor as a 6×6 matrix), and density, ρ, of Earth materials vary with pressure, P, temperature, T, and chemistry. Knowledge of the effect of pressure on the elasticity of the clinopyroxenes is currently lacking (Mainprice, 2007).

The monoclinic (space group $C2/c$) clinopyroxenes diopside ($CaMgSi_2O_6$) and jadeite ($NaAlSi_2O_6$) share the same chain silicate structure and, at elevated temperature, form a solid solution. Up to 20% of fertile upper mantle peridotite is formed from diopside rich clinopyroxenes which are lost on partial melting (Herzberg, 1995), and these minerals form the majority component of subducted Mid-Ocean Ridge Basalt (MORB) to ∼10 GPa where they dissolve into garnet (Irifune et al., 1986; Irifune and Ringwood, 1993). However, the elastic constants of diopside and jadeite are only known from experiments at low pressure. C_{ij} for nearly end-member diopside and jadeite have been determined under ambient conditions from Brillouin spectroscopy by Levien et al. (1979) and Kandelin and Weidner (1988), respectively. The elastic properties of pyroxenes with intermediate compositions have been measured by Bhagat et al. (1992) and Collins and Brown (1998), who found that most (but not all) of the individual elastic constants follow a linear mixing law across the compositional range. This analysis was extended by Isaak and Ohno (2003) who measured the elastic constants of a chrome-diopside which, when projected

onto the jadeite-diopside join, plot close to the predicted linear relationship for all of the elastic constants apart from C_{66}, C_{13} and C_{15}. In light of this, Isaak and Ohno (2003) argue that these elements of the elastic constants tensor of end-member diopside warrant revisiting.

The effect of temperature on the elasticity of diopside has been measured by Isaak et al. (2006), who found that the temperature dependence was small. Indeed, the temperature induced softening of the polycrystalline averages for the bulk and shear moduli were the smallest measured for any of the main mantle minerals. The individual measured values of $(\partial C_{ij}/\partial T)_P$ indicate that the elastic constants generally soften by $\sim$10% with a temperature increase of 1000 K, but it is notable that C_{15}, C_{25} and C_{46} significantly stiffen with increasing temperature. Recently, Li and Neuville (2010) have measured the velocity of ultrasonic waves propagating through polycrystalline aggregates of diopside as a function of temperature and pressure to 1073 K and 8.4 GPa. This data permits the recovery of the average bulk and shear moduli along with their temperature and pressure derivatives. The measured temperature derivatives are within error of the averaged values of Isaak et al. (2006) and the bulk modulus and its pressure derivative is broadly compatible with scattered results from compression experiments (Levien and Prewitt, 1981; Zhang et al., 1997; Zhao et al., 1998; Tribaudino et al., 2000; Thompson and Downs, 2008). Although these data can be used to interpret the seismic wave velocities in much of the upper mantle, averaged elastic moduli are not sufficient for the analysis of seismic anisotropy: the pressure derivatives of the individual elements of C_{ij} are required.

In the absence of experimental data, it is reasonable to turn to atomic scale simulation to provide knowledge of the mineral properties needed to interpret

seismological observations. In a recent review, Mainprice (2007) noted the lack of measurements of $(\partial C_{ij}/\partial P)_T$ for diopside and recommended the use of the results of an atomic scale study by Matsui and Busing (1984). This study used interatomic potentials derived from the experimental structure and elastic constants of diopside to describe the forces acting between model atoms. In detail, the potential model predates many important advances towards transferable models for atomic interactions in silicates (e.g. polarisable shell models, suitably flexible SiO_4 groups; see Dove, 1989, for further discussion). A further difficulty with the use of these results is more fundamental to any interatomic potential — however well the model reproduces known experimental data, it is not easy to predict the limits beyond which the results of this kind of extrapolative model become unreliable. Perhaps in recognition of this Matsui and Busing (1984) limited their calculations to only 5 GPa; some diopside is expected to persist in the mantle to $\sim$20 GPa. In the current work the elastic constants of diopside and jadeite were predicted at the atomic scale whilst avoiding the use of a parameterised model to describe the interactions between atoms. Instead, the interatomic interactions were calculated by considering the distribution and interactions of the electrons in the system. This sidesteps the dangers associated with the extrapolation of a simple potential model fitted to selected experimental results.

2 Methodology

Density functional theory (DFT: Hohenberg and Kohn, 1964; Kohn and Sham, 1965) was used to calculate the elastic constants and seismic wave velocities of diopside and jadeite to elevated pressure. DFT allows the calculation of

the forces acting between atoms, and thus the equilibrium structure and derived properties, of materials by finding an approximate solution to the many body time-independent Schrödinger equation for a collection of electrons in the potential field of their nuclei. Importantly, this is done without the need to evaluate the full many-body wave function for a system of interacting electrons. Instead, all ground state properties, such as the cohesive energy, are functionals of the electron density. The current study builds on the previous calculations of the athermal equation of state of diopside reported by Walker et al. (2008). In common with the previous study, the semi-local gradient corrected (GGA) functional of Perdew et al. (1996) was used as an approximation to the (unknown) exact exchange correlation functional. Ultrasoft pseudopotentials were used to describe the core electrons and nuclei with electrons in the 2s, 2p, and 3s levels in Na, the 3s and 3p levels in Al, the 2s and 2p levels in O, the 2p and 3s levels in Mg, the 3s, 3s and 3p levels in Si, and the 3s, 3p and 4s levels in Ca treated as belonging to the valence. Further details of the pseudopotentials can be found in Walker et al. (2008). The valance electrons were described using a planewave basis expansion that includes all waves whose kinetic energy is less than a cutoff energy threshold. Following convergence testing (see Walker et al., 2008, and the Supplementary Information) a planewave cutoff of 700 eV was used for all calculations. The Brillouin zone was sampled with a $2 \times 2 \times 3$ Monkhorst-Pack grid (Monkhorst and Pack, 1976). All calculations were performed using version 5.0.2 of the CASTEP code (Clark et al., 2005).

There are a number of approaches that can be taken to extract elastic constants from atomic scale calculations. Perhaps the most direct approach involves writing the elastic constants in terms of the second derivative of the

energy with respect to the lattice parameters (Nye, 1985), calculating the derivatives and from these C_{ij}:

$$C_{ij} = \frac{1}{V} \frac{\partial^2 H}{\partial \varepsilon_i \partial \varepsilon_j} \bigg|_{P,T=0}, \tag{1}$$

where V is the unit cell volume, H is the unit cell enthalpy and ε is a strain (expressed as a 6-element vector). This approach is common in calculations using parameterised models for the interatomic potential where the required second derivatives are readily available (Gale and Rohl, 2003). The derivatives can also be calculated using density functional perturbation theory (Hamann et al., 2005), but the use of ultrasoft pseudopotentials make the implementation of this approach particularly challenging. Examples of the use of this method for Earth materials are comparatively sparse, but include Caracas and Bagigan (2009) and Caracas and Boffa Ballaran (2010). A common alternative approach is used here. Instead of calculating the second derivatives of the energy for an undeformed crystal, small strains are imposed on the equilibrium lattice vectors and the resulting stresses are calculated. If the strains are sufficiently small to ensure the deformation is in the linear regime, Hooks law is valid and the constants of proportionality between the stresses, σ, and strains are elastic constants:

$$\sigma_i = C_{ij} \varepsilon_j, \tag{2}$$

which can be calculated by linear regression. There are many examples of this approach in the literature with Wentzcovitch et al. (1995, 2004), Karki et al. (1999), Stackhouse et al. (2005), Perger et al. (2009), Mookherjee and Steinle-Neumann (2009) and many others using this method with DFT to evaluate elastic constants of Earth materials (see Karki et al., 2001).

Practically, calculating the elastic constants involves a number of steps. First the equilibrium lattice vectors and atomic positions are determined at the pressure of interest by performing an energy minimisation allowing the atomic positions and lattice vectors to vary. It is critically important that the minimum energy configuration is determined accurately otherwise the stresses calculated in the next step can be significantly in error. For the calculations reported here, this was achieved by tightening the various convergence criteria used to stop the geometry optimisation algorithm compared to the settings used for the athermal equation of state calculations. The stopping condition was that the change in total energy, ionic forces, ionic displacements and all components of the calculated stress were less than 2×10^{-7} eV/atom, 1×10^{-3} eV/Å, 1×10^{-3} Å and 1×10^{-3} GPa, respectively, and that these conditions were met for at least two consecutive optimisation steps. This, in turn, required tight convergence criteria for the electronic optimiser (total energy change less than 1×10^{-8} eV for three consecutive steps). The second step is to strain the unit cell by a small amount and perform a second geometry optimisation, this time with fixed lattice vectors. Once the minimum energy atomic co-ordinates have been found the constant of proportionality relating an element of the stress tensor of the strained cell with an element of the applied strain tensor is an elastic constant. By applying several different strains, the full elastic constants tensor can be determined. Symmetry is used to speed up both types of geometry optimisation calculation. In the first stage symmetry operators of the $C2/c$ are applied, in the second stage only the smaller set of operators which remain after the application of the homogeneous strain are used.

Symmetry means that the elasticity of monoclinic diopside and jadeite can be described by 13 independent elastic constants rather than the 21 constants

needed in in the most general triclinic case. This, in turn, means that all the elastic constants can be extracted from four patterns of strain, rather than the six strain patterns needed for the general case. The four chosen strain patterns (others are possible) are:

$$\varepsilon^1 = \pm\delta \begin{pmatrix} 1 & 0 & 0 \\ 0 & 0 & \frac{1}{2} \\ 0 & \frac{1}{2} & 0 \end{pmatrix}; \varepsilon^2 = \pm\delta \begin{pmatrix} 0 & \frac{1}{2} & 0 \\ \frac{1}{2} & 0 & 0 \\ 0 & 0 & 1 \end{pmatrix}; \tag{3}$$

$$\varepsilon^3 = \pm\delta \begin{pmatrix} 0 & 0 & 0 \\ 0 & 1 & 0 \\ 0 & 0 & 0 \end{pmatrix}; \varepsilon^4 = \pm\delta \begin{pmatrix} 0 & 0 & \frac{1}{2} \\ 0 & 0 & 0 \\ \frac{1}{2} & 0 & 0 \end{pmatrix};$$

where a superscript is used to denote the pattern index and δ is the strain magnitude. For each pattern three positive and three negative strain magnitudes are imposed and linear regression is used to find the elastic constants from Equation 2. The use of six different strains for each pattern allows an estimate of the error on each elastic constant arising from inaccuracies in the calculated stresses (arising, for example, from the finite convergence criteria) and any non-linearity in the stress — strain curve. These errors can be propagated into values derived from the elastic constants, such as the polycrystalline averaged bulk and shear moduli. The fitting errors increase if the applied strain is too large and Hook's law begins to break down or if the strains are too small and the calculated stresses become small compared to the errors due to the

chosen convergence criteria. In the current work, it was found that the errors were acceptably small if strains equivalent to changing the length of a lattice vector by ± 0.0333, ± 0.0666 and ± 0.1 Å were used.

3 Results

The evolution of the calculated unit cell volume of jadeite and diopside as a function of pressure is shown in Figure 1 alongside a range of experimental measurements. It is immediately apparent that at all pressures the cell volume of both minerals is overestimated by the DFT calculations. This is the result of a known defect of the GGA which commonly "under-binds" giving bond lengths that are too long, cell volumes that are too large, phonon frequencies that are too small and elastic constants that are too soft. However, the derivatives of the energy with inter-atomic separation are typically well reproduced. This allows the application of an empirical correction to the applied pressure to correct for the under-binding, yielding results which can more easily be compared with experiment (e.g. Vanderbilt, 1998; Oganov et al., 2001). In the previous study of diopside Walker et al. (2008) used empirical pressure correction of 4.66 GPa. For jadeite, the necessary pressure correction is found to be 4.30 GPa. Once this correction has been made, the DFT results are in good agreement with the experimental results with calculated cell volumes coinciding with the experimental measurements across the whole pressure range (Figure 1). The results of fitting third-order Birch-Murgahan equations of state to these data are $V_0 = 401.3$ Å^3, $K_0 = 128.8$ GPa and $K_0' = 3.8$ for jadeite and $V_0 = 439.1$ Å^3, $K_0 = 122.0$ GPa and $K_0' = 4.7$ for diopside (Walker et al., 2008). For jadeite, experimental data gives $V_0 = 402.26 \pm 0.02$

Å^3, $K_0 = 134.0 \pm 0.7$ GPa and $K_0' = 4.4 \pm 0.1$ (Nestola et al., 2006) and $K_0 = 124.5 \pm 4.0$ assuming K_0' of 5.0 (Zhao et al., 1997) with the differences attributable to the trade-off between V_0, K_0 and K' and the difference in pressure range between the data sets.

A more stringent test of the calculations is to compare the atomic positions and lattice vectors with experimental measurements. For diopside agreement is excellent and is described in Walker et al. (2008). For jadeite the recent low temperature structure refinement of neutron powder diffraction data performed by Knight and Price (2008) can be used as a reference. Because this is at very low temperature (1.5 K for the lattice vectors and 2.4 K for the atomic positions), vibrational corrections to the results from the static DFT calculations can be neglected. After the pressure correction for jadeite, all atomic positions agree with experimental data to better than 0.002 fractional units ($\sim$0.02 Å) and length of the cell parameters, and β angle, are consistent with the experimental measurements to $\sim$0.01 Å or $\sim$0.1°. Further details, including a full analysis of the evolution of the jadeite crystal structure with pressure, are given in the Supplementary Information.

The calculated elastic constants of diopside and jadeite are compared to ambient pressure experiments in Tables 1 and 2. DFT results are presented at 0 GPa and at an applied pressure of 4.66 or 4.30 GPa to include the pressure correction. The calculated results are in much better agreement with the experimental data once the empirical pressure correction has been made, further supporting the application of such a correction. Compared to the experimental results of Isaak and Ohno (2003), the DFT calculations generally overestimate the stiffness of diopside (the exceptions are C_{44}, where the DFT result lies between the result of Isaak and Ohno (2003) and Levien et al. (1979), C_{25} and

C_{46}, where the pressure derivative is negative). The overestimate is generally less than 10 GPa and of a similar in magnitude to the differences between the experimental results of Isaak and Ohno (2003) and Levien et al. (1979). However, C_{12}, C_{13}, C_{35} and, particularly, C_{11} are more dramatically overestimated with deviations from the results of Isaak and Ohno (2003) of between 10 and 16 GPa. For jadeite, almost all the elastic constants calculated using DFT are within error of the experimental results of Kandelin and Weidner (1988) with the three exceptions being C_{11}, C_{55} and C_{35} where DFT overestimates the elastic constants by 9.4, 6.4 and 13.5 GPa, respectively. For comparison, 0 GPa elastic constants of both minerals calculated using the local density approximation (LDA) are also presented. As expected, these are generally stiffer than the experimental values and the LDA and GGA tend to bracket the observed elasticity. Robust conclusions regarding the value of LDA and GGA estimates of the elastic constants of low symmetry minerals are hard to make from this limited dataset. However, the case of jadeite is interesting: here the uncorrected LDA and pressure corrected GGA calculations give very good estimates of the isotropic (see below) bulk modulus. However, while the shear modulus is well reproduced by the GGA calculations, it is overestimated by the LDA calculations. This cannot be corrected by changing the pressure without detriment to the estimate of the bulk modulus.

A starting point for the analysis of how clinopyroxenes would affect seismic velocities is to consider the elastic properties of polycrystalline samples where the individual crystals are randomly oriented. Such a composite is elastically isotropic and can be described by two elastic parameters, e.g. the effective bulk, K, and shear, G, moduli. There are multiple methods for finding the two moduli which make use of different assumptions for the distribution of

stress and strain in the polycrystalline sample. The upper Voigt bound (K^v and G^v) is found by assuming the strain is uniform throughout the aggregate while the lower Reuss bound (K^r and G^r) assumes the stress is uniform; the arithmetic mean (the Voigt-Reuss-Hill average, K^{vrh} and G^{vrh}) of these two limits is often a good approximation of the physically realised situation (Hill, 1952; Chung and Buessem, 1967). Values for the averaged moduli are given in Tables 1 and 2 where the agreement between the experimental and DFT averages are acceptable but the overestimate of C_{11} in diopside results in a $\sim$10% overestimate of its bulk modulus.

The evolution of the calculated elastic constants of diopside with pressure are reported in Figure 2 and in tabular form in the Supplementary Information. It is apparent that several of the shear moduli (C_{15}, C_{25}, C_{35} and C_{46}) have negative pressure derivatives. Indeed C_{25} and C_{46} become negative by 20 GPa and C_{15} approaches zero. It is worth noting that the modelled crystal remains elastically stable at all pressures (C_{ij} is positive definite, even if C_{15} becomes negative, see Born and Huang, 1954, page 141). The effect of pressure on the polycrystalline average bulk and shear moduli can be compared with the recent experimental results of Li and Neuville (2010). Taking the difference between the DFT results at 0 GPa and 5 GPa yields values of 4.7 and 1.2 for $(\partial K/\partial P)_T$ and $(\partial G/\partial P)_T$, respectively. These values are in good agreement with those of Li and Neuville (2010), who find 4.9 and 1.6, respectively. The equivalent data for jadeite is also reported in Figure 2. The elastic constants show the same softening of C_{15} and C_{46} with increasing pressure but in contrast to diopside C_{25} stiffens while C_{35} stiffens to a maximum at around 10 GPa before beginning to soften.

Combining the elastic constants with the density calculated from the ather-

mal equation of state allows the phase velocities of the three seismic waves to be calculated as a function of propagation direction by finding solutions to the Christoffel equation (e.g. Mainprice, 2007). In the current work, this is performed using a Matlab program based on the algorithm presented by Mainprice (1990). For each direction, the three velocities are assigned to the fast, V_{s1}, and slow, V_{s2}, quasi-S waves and a quasi-P wave, V_p. These wave velocities are summarised in Figure 3 for diopside and Figure 4 for jadeite where pole figures describe the distribution of P-wave velocities, the S-wave anisotropy, $aV_s = (V_{s1} - V_{s2})/\frac{1}{2}(V_{s1} + V_{s2})$, and the fast S-wave polarisation direction as a function of propagation direction. It can be seen that the P-wave anisotropy and maximum S-wave anisotropy of diopside is larger than that of jadeite at low pressure, with the anisotropies becoming more similar by 20 GPa. The pattern of anisotropy for the two minerals is, however, quite different at all pressures. Diopside possesses a distinct aV_s minimum in the plane containing the a and c lattice vectors, which is not expressed by jadeite.

4 Discussion

By any measure the clinopyroxenes are the most elastically anisotropic of the upper mantle minerals. Two ways of describing the total anisotropy of a low symmetry crystal are the general anisotropy index ($\mathrm{A}^\star = V^2_{s(max)}/V^2_{s(min)}$, where the maximum and minimum phase velocities are found from a search over all propagation directions, Ledbetter and Miglion, 2006) and the universal anisotropy index (A^U, derived from the Voigt and Reuss estimates of the isotropic average bulk and shear moduli, Ranganathan and Ostoja-Starzewski, 2008). By both measures diopside ($\mathrm{A}^\star = 1.91$, $\mathrm{A}^U = 0.495$) and jadeite ($\mathrm{A}^\star =$

1.86, $A^U = 0.334$) are more anisotropic than enstatite ($A^\star = 1.31$, $A^U = 0.074$, Weidner et al., 1978) or olivine ($A^\star = 1.56$, $A^U = 0.23$, Abramson et al., 1997). A more geophysically relevant measure is the maximum value of aV_s found by searching over all wave propagation directions for the two minerals. For diopside the maximum value of aV_s at 0 GPa is 29% (Figure 3) while for jadeite it is 20% (Figure 4); both values are considerably higher than those of olivine and enstatite which are 18% and 11%, respectively.

The DFT calculations reveal that, in common with the effect of temperature, the effect of pressure on the elastic constants tensor of diopside and jadeite is rather small. For diopside all measures of total anisotropy decrease slowly from 0 to 20 GPa where $A^\star = 1.74$, $A^U = 0.312$ (values at other pressures are given in the Supplementary Information) and the maximum value of aV_s is 25%. This is in dramatic contrast to the linear extrapolation of the data of Matsui and Busing (1984) which results in an increase in the anisotropy. By 20 GPa such an extrapolation yields very high anisotropy for diopside with $A^\star = 2.72$, $A^U = 1.72$ and a maximum value for aV_s of 43%. Jadeite behaves differently to diopside. The anisotropy of jadeite slowly increases to a maximum at around 10 GPa before beginning to decrease.

The high elastic anisotropy of diopside will have an effect on the bulk anisotropy of the deforming upper mantle. Without a detailed understanding of the active slip systems and deformation mechanisms of diopside, and a realistic model of inter-grain interactions the details are hard to predict. However, it is worth noting that the inclusion of enstatite in a simple two dimensional model of anisotropy generation around a mid-ocean ridge resulted in significant changes to the predicted bulk anisotropy (Kaminski et al., 2004). A useful illustration of the kind of effect clinopyroxenes may have of the seismic anisotropy is pro-

vided by considering a shear wave passing through the oceanic crust forming the upper layer of a subducting slab. Between depths of about 150 and 400 km, the basaltic layer consists of eclogite, a mixture of clinopyroxene and garnet (Irifune et al., 1986; Irifune and Ringwood, 1993). A first approximation (and upper bound) of the magnitude of the shear wave splitting caused by this layer can be found by assuming the crust consists of a 5 - 10 km thick layer of diopside completely aligned by deformation. Furthermore, if the crystals are assumed to align with (010) parallel to the slab and the wave is assumed to propagate in the direction perpendicular to the slab, it is possible to calculate the expected shear wave splitting due to the diopside rich layer. In such a model the shear wave splitting increases dramatically with increasing depth (Table 3) with 0.2 seconds of delay being possible. Such splitting is not insignificant. S-wave splitting from local events around northeastern Japan (Nakajima and Hasegawa, 2004), the New Zealand (Morley et al., 2006) and the Java-Sumatra subduction zones (Hammond et al., 2010) are typically up to 0.5 seconds. Two effects that are excluded from this simple analysis are the increasing garnet component with depth and the corresponding increase in the jadeitic component of the clinopyroxene. Both of these effects will diminish the shear wave splitting. On the other hand, geometrical effects can only increase the apparent thickness of the crustal layer and thus act to increase the observed splitting. Perhaps the most interesting feature of this result is that the shear anisotropy in the [010] direction doubles between 5 and 15 GPa while all estimates of the anisotropy of the elastic constants tensor as a whole show a small decrease in anisotropy. Changes in shear wave splitting in the [010] direction are driven by a distortion of the distribution of fast and slow shear wave velocities rather than a major change in their relative magnitudes.

5 Conclusions

Because of the low crystal symmetry the effect of pressure on the individual elastic constants of jadeite and diopside is difficult to determine experimentally. For diopside, previous results based on interatomic potentials fitted to room pressure elastic constants (Matsui and Busing, 1984) give an adequate description at low pressures but become very anisotropic at transition zone pressures. In this work elastic constants have been calculated using an electronic structure based approach which does not require experimental input beyond an approximate initial crystal structure. For both minerals, the elastic constants at 0 GPa are in good agreement with values derived from experiment (with the notable exception of C_{11}, which is significantly overestimated). Extending the calculations to 20 GPa shows that the anisotropy decreases slightly with pressure. Despite this decrease in total anisotropy, the expected shear wave splitting for waves propagating perpendicular to the (010) plane increases rapidly with pressure. The effect of the inclusion of clinopyroxenes in models of seismic anisotropy of the upper mantle is thus likely to be more complex than anticipated from straightforward estimates of the total anisotropy of these minerals.

6 Acknowledgments

This research was supported by a NERC Postdoctoral Research Fellowship (NE/E012922/2) and made use of the facilities of HECToR, the UK's national high-performance computing service, which is provided by UoE HPCx Ltd at the University of Edinburgh, Cray Inc and NAG Ltd, and funded by the

Office of Science and Technology through EPSRC's High End Computing Programme.

References

Abramson, E. H., Brown, J. M., Slutsky, L. J., Zaug, J., 1997. The elastic constants of San Carlos olivine to 17 GPa. Journal of Geophysical Research 102, 12253 – 12263.

Bhagat, S. S., Bass, J. D., Smyth, J. R., 1992. Single-crystal elastic properties of omphaite-C2/c by Brillouin spectroscopy. Journal of Geophysical Research 97, 6843 – 6848.

Born, M., Huang, K., 1954. Dynamical Theory of Crystal Lattices. Oxford University Press.

Caracas, R., Bagigan, E. J., 2009. Elasticity and Raman spectra of $MgAl_2O_4$ spinel from density functional perturbation theory. Physics of the Earth and Planetary Interiors 174, 113 – 121.

Caracas, R., Boffa Ballaran, T., 2010. Elasticity of $(K,Na)AlSi_3O_8$ hollandite from lattice dynamics calculations. Physics of the Earth and Planetary Interiors 181, 21 – 26.

Chung, D. H., Buessem, W. R., 1967. The Voigt–Reuss–Hill approximation and elastic moduli of polycrystalline MgO, CaF_2, β-ZnS, ZnSe, and DdTe. Journal of Applied Physics 38, 2535 – 2540.

Clark, S. J., Segall, M. D., Pickard, C. J., Hasnip, P. J., Probert, M. I. J., Refson, K., Payne, M. C., 2005. First principles methods using castep. Zeitschrift fuer Kristallographie 220, 567 – 570.

Collins, M. D., Brown, J. M., 1998. Elasticity of an upper mantle clinopyroxene. Physics and Chemistry of Minerals 26, 7 – 13.

Dove, M. T., 1989. On the computer modeling of diopside: toward a transferable potential for silicate minerals. American Mineralogist 74, 774–779.

Gale, J. D., Rohl, A. L., 2003. The general utility lattice program (GULP). Molecular Simulation 29 (5), 291 – 341.

Hamann, D. R., Wu, X., Rabe, K. M., Vanderbilt, D., 2005. Metric tensor formulation of strain in denity-functional pertubation theory. Physical Review B 71, 035117.

Hammond, J. O. S., Wookey, J., Kaneshima, S., Inoue, T., Yamashina, T., Harjadi, P., 2010. Systematic variation in anisotropy beneath the mantle wedge in the Java–Sumatra subduction system from shear-wave splitting. Physics of the Earth and Planetary Interiors 178, 189 – 201.

Herzberg, C., 1995. Phase equilibria of common rocks in the crust and mantle. In: Ahrens, T. J. (Ed.), Rock physics and phase relations: a handbook of physical constants. Vol. 3 of AGU Reference Shelf. American Geophysical Union, pp. 166 – 177.

Hill, R., 1952. The elastic behaviour of a crystalline aggregate. Proceedings of the Physics Society A 65, 349 – 354.

Hohenberg, P., Kohn, W., 1964. Inhomogeneous electron gas. Physical Review 136 (3B), 864 – 871.

Irifune, T., Ringwood, A. E., 1993. Phase transformations in subducted oceanic crust and buoyancy relationships at depths of 600–800 km in the mantle. Earth and Planetary Science Letters 117, 101 – 110.

Irifune, T., Sekine, T., Ringwood, A. E., Hibberson, W. O., 1986. The eclogite-garnetite transformation at high pressure and some geophysical implicaions. Earth and Planetary Science Letters 77, 245 – 256.

Isaak, D. G., Ohno, I., 2003. Elastic constants of chrome-diopside: application of resonany ultrasound spectroscopy to monoclinic single-crystals. Physics

and Chemistry of Minerals 30, 430 – 439.

Isaak, D. G., Ohno, I., Lee, P. C., 2006. The elastic constants of monoclinic single-crystal chrome-diopside to 1,300 K. Physics and Chemistry of Minerals 32, 691 – 699.

Kaminski, E., Ribe, N. M., Browaeys, J. T., 2004. D-Rex, a program for calculation of seismic anisotropy due to crystal lattice preferred orientation in the convective upper mantle. Geophysical Journal International 158, 744 – 752.

Kandelin, J., Weidner, D. J., 1988. The single-crystal elastic properties of jadite. Physics of the Earth and Planetary Interiors 50, 251 – 260.

Karki, B. B., Wentzcovitch, R. M., de Gironcoli, S., Baroni, S., 1999. First-principles determination of elastic anisotropy and wave velocities of MgO at lower mantle conditions. Science 286, 1705 – 1707.

Karki, B. B., Stixrude, L., Wentzcovitch, R. M., 1999. High-pressure elastic properties of major materials of Earth's mantle from first principles. Reviews of Geophysics 39, 507 – 534.

Knight, K. S., Price, G. D., 2008. Powder neutron-diffraction studies of clinopyroxenes. I. The crystal structure and thermoelastic properties. The Canadian Mineralogist 46, 1593 – 1622.

Kohn, W., Sham, L. J., 1965. Self-consistent equations including exchange and correlation effects. Physical Review 140 (4A), 1133 – 1138.

Ledbetter, H., Miglion, A., 2006. A general elastic-anisotropy measure. Journal of Applied Physics 100, 063516.

Levien, L., Prewitt, C. T., 1981. High-pressure structural study of diopside. American Mineralogist 66, 315–323.

Levien, L., Weidner, D. J., Prewitt, C. T., 1979. Elasticity of diopside. Physics and Chemistry of Minerals 4, 105 – 113.

Li, B., Neuville, D. R., 2010. Elasticity of diopside to 8 GPa and 1073K and implications for the upper mantle. Physics of the Earth and Planetary Interiors 183, 398 – 493.

Mainprice, D., 1990. A fortran program to calculate seismic anisotropy from the lattice preferred orientation of minerals. Computers and Geosciences 16, 385 – 393.

Mainprice, D., 2007. Seismic anisotropy of the deep earth from a mineral and rock physics perspective. In: Price, G. D. (Ed.), Treatise on Geophysics. Mineral Physics. Vol. 2. Elsevier, pp. 437 – 491.

Matsui, M., Busing, W. R., 1984. Calculation of the elastic constants and high-pressure properties of diopside, $CaMgSi_2O_6$. American Mineralogist 69, 1090–1095.

McCormick, T. C., Hazen, R. M., Angel, R. J., 1989. Compressibility of omphacite to 6-Kbar: Role of vacancies. American Mineralogist 74, 1287 – 1292.

Monkhorst, H. J., Pack, J. D., 1976. Special points for Brillouin-zone integrations. Physical Review B 13, 5188 – 5192.

Mookherjee, M., Steinle-Neumann, G., 2009. Detecting deeply subducted crust from the elasticity of hollandite. Earth and Planetary Science Letters 288, 349 – 358.

Morley, A. M., Stuart, G. W., Kendall, J.-M., Reyners, M., 2006. Mantle wedge anisotropy in the Hikurangi subduction zone, central North Island, New Zealand. Geophysical Research Letters 33, L05301.

Nakajima, J., Hasegawa, A., 2004. Shear-wave polarization anisotropy and subduction-induced flow in the mantle wedge of northeastern Japan. Earth and Planetary Science Letters 225, 365 – 377.

Nestola, F., Boffa Ballaran, T., Liebske, C., Bruno, M., Tribaudino, M., 2006.

498 High-pressure behaviour along the jadeite $NaAlSi_2O_6$–aegirine $NaFeSi_2O_6$
499 solid solution up to 10 GPa. Physics and Chemisty of Minerals 33, 417 –
500 425.
501 Nye, J. F., 1985. Physical Properties of Crystals: Their Representation by
502 Tensors and Matrices. Oxford University Press.
503 Oganov, A. R., Brodholt, J. P., Price, G. D., 2001. Ab initio elasticity and
504 thermal equation of state of $MgSiO_3$ perovskite. Earth and Planetary Sci-
505 ence Letters 184, 555 – 560.
506 Perdew, J. P., Burke, K., Emzerhof, M., 1996. Generalized gradient approxi-
507 mation made simple. Physical Review Letters 77, 3865 – 3868.
508 Perger, W. F., Criswell, J., Civalleri, B., Dovesi, R., 2009. Ab-initio calculation
509 of elastic constants of crystalline systems with the crystal code. Computer
510 Physics Communications 180, 1753 – 1759.
511 Ranganathan, S. I., Ostoja-Starzewski, M., 2008. Universal elastic anisotropy
512 index. Physical Review Letters 101, 055504.
513 Stackhouse, S., Brodholt, J. P., Wookey, J., Kendall, J.-M., Price, G. D.,
514 2005. The effect of temperature on the seismic anisotropy of the perovskite
515 and post-perovskite polymorphs of $MgSiO_3$. Earth and Planetary Science
516 Letters 230, 1 – 10.
517 Thompson, R. M., Downs, R. T., 2008. The crystal structure of diopside at
518 pressure to 10 GPa. American Mineralogist 93, 177 – 186.
519 Tribaudino, M., Prencipe, M., Bruno, M., Levy, D., 2000. High-presure be-
520 haviour of Ca-rich $C2/c$ clinopyroxenes along the join diopside-enstatite
521 ($CaMgSi_2O_6$). Physics and Chemistry of Minerals 27, 656 – 664.
522 Vanderbilt, D., 1998. First-principles theory of structural phase transitions in
523 cubic perovskites. Journal of the Korean Physical Society 32, S103 – S106.
524 Walker, A. M., Tyer, R. P., Bruin, R. P., Dove, M. T., 2008. The compressibil-

ity and high pressure structure of diopside from first principles simulation. Physics and Chemistry of Minerals 35, 359 – 366.

Weidner, D. J., Wang, H., Ito, J., 1978. Elasticity of orthoenstatite. Physics of the Earth and Planetary Interiors 17, 7 – 13.

Wentzcovitch, R. M., Ross, N. L., Price, G. D. 1995. Ab initio study of $MgSiO_3$ and $CaSiO_3$ at lower-mantle pressures. Physics of the Earth and Planetary Interiors 90, 101 – 112.

Wentzcovitch, R. M., Karki, B. B., Cococcioni, M., de Gironcoli, S. 2004. Thermoelastic properties of $MgSiO_3$-perovskite: Insights on the nature of the Earths lower mantle. Physical Review Letters 92, 018501.

Zhang, L., Ahsbahs, H., Hafner, S. S., Kutoglu, A., 1997. Single-crystal compression and crystal structure of clinopyroxene up to 10 GPa. American Mineralogist 82, 245–258.

Zhao, Y., Von Dreele, R. B., Shankland, T. J., Weidner, D. J., Zhang, J., Wang, Y., Gasparik, T., 1997. Thermoelastic equation of state of jadeite $NaAlSi_2O_6$: An energy-dispersive Reitveld refinement study of low symmetry and multiple phases diffraction. Geophysical Research Letters 24, 5–8.

Zhao, Y., Von Dreele, R. B., Zhang, J. Z., Weidner, D. J., 1998. Thermoelastic equation of state of monoclinic pyroxene: $CaMgSi_2O_6$ diopside. Review of High Pressure Science and Technology 7, 25 – 27.

Table 1
Elastic constants (in GPa) of diopside from GGA calculations at 0 GPa and 4.66 GPa compared with experimental data. [a]data for $Di_{93}Hd_9Jd_3Cr_3Ts_{12}$ from resonant ultrasound spectroscopy results of Isaak and Ohno (2003). [b]data for $Ca_{0.99}Na_{0.02}Mg_{0.9}Al_{0.01}Fe_{0.02}Si_{1.99}0_6$ from Brillouin scattering results of Levien et al. (1979).

	Chrome-diopside[a]	diopside[b]	LDA 0 GPa	GGA 0 GPa	GGA 4.66 GPa
C_{11}	228.1±1.0	223±2	242.6±1.4	212.3±1.1	243.7±1.4
C_{22}	181.1±0.6	171±2	183.7±1.2	158.0±1.1	184.1±1.2
C_{33}	245.4±1.3	235±2	254.3±2.5	226.3±1.5	251.0±1.8
C_{44}	78.9±0.3	74±1	79.8±0.3	65.3±0.6	76.9±0.4
C_{55}	68.2±0.2	67±1	73.8±1.1	61.9±0.1	69.3±0.1
C_{66}	78.1±0.2	66±2	84.5±0.9	69.3±0.5	80.6±0.7
C_{12}	78.8±0.5	77±3	90.5±0.8	69.8±0.7	91.2±0.7
C_{13}	70.2±0.7	81±2	78.8±1.1	60.6±0.9	80.5±1.1
C_{23}	61.1±0.7	57±2	62.5±0.7	50.7±0.4	68.0±0.7
C_{15}	7.9±0.5	17±1	9.3±0.6	15.4±0.3	9.1±0.3
C_{25}	5.9±0.5	7±2	5.4±0.6	10.0±0.1	4.5±0.1
C_{35}	39.7±0.4	43±1	51.8±0.4	54.9±0.3	50.9±0.1
C_{46}	6.4±0.2	7.3±0.9	3.6±0.4	10.8±0.4	3.9±0.2
K^{vrh}	116.5±0.9	113±1	122.6±0.6	99.8±0.4	124.3±0.6
G^{vrh}	72.8±0.4	67±0.6	74.6±0.4	63.5±0.2	71.7±0.2

Table 2
Elastic constants (in GPa) of jadeite compared with experimental data from Brillouin spectroscopy of Kandelin and Weidner Kandelin and Weidner (1988).

	Kandelin and Weidner (1988)	LDA 0GPa	GGA 0 GPa	GGA 4.30 GPa
C_{11}	274±4	285.4±2.3	243.6±2.5	283.4±2.6
C_{22}	253±4	262.3±1.8	228.1±1.7	252.6±1.7
C_{33}	282±3	290.9±2.1	266.2±2.4	281.8±0.9
C_{44}	88±2	91.4±0.7	79.5±0.4	86.7±0.2
C_{55}	65±4	74.3±0.4	64.6±0.4	71.4±0.1
C_{66}	94±2	102.1±1.3	85.7±1.2	96.5±1.4
C_{12}	94±2	94.4±1.0	77.4±0.9	93.3±0.8
C_{13}	71±8	68.1±1.2	56.1±1.0	72.5±1.2
C_{23}	82±4	79.8±0.3	73.5±0.3	81.8±0.9
C_{15}	4±3	5.0±0.5	11.7±0.9	4.4±0.4
C_{25}	14±4	14.6±0.3	14.0±0.2	14.0±0.1
C_{35}	28±3	43.0±0.9	37.8±0.6	41.5±0.6
C_{46}	13±1	12.2±0.1	14.5±0.3	11.9±1.4
K^{vrh}	143±2	143.9±0.6	124.5±0.6	142.8±0.7
G^{vrh}	85±2	90.7±0.4	78.9±0.3	86.5±0.3

Table 3
Simple model of shear-wave splitting for eclogite layer on subducting slab. δt is the calculated delay time between the fast and slow shear-wave arrival. See text for details.

Pressure (GPa)	$V_{s1}^{[010]}$ (km/s)	$V_{s2}^{[010]}$ (km/s)	$aV_s^{[010]}$ (%)	δt (5 km) (s)	δt (10 km) (s)
5	5.21	4.88	6.5	0.06	0.13
10	5.42	4.83	11.5	0.11	0.23
15	5.54	4.90	12.3	0.12	0.24
20	5.59	4.62	19.0	0.19	0.38

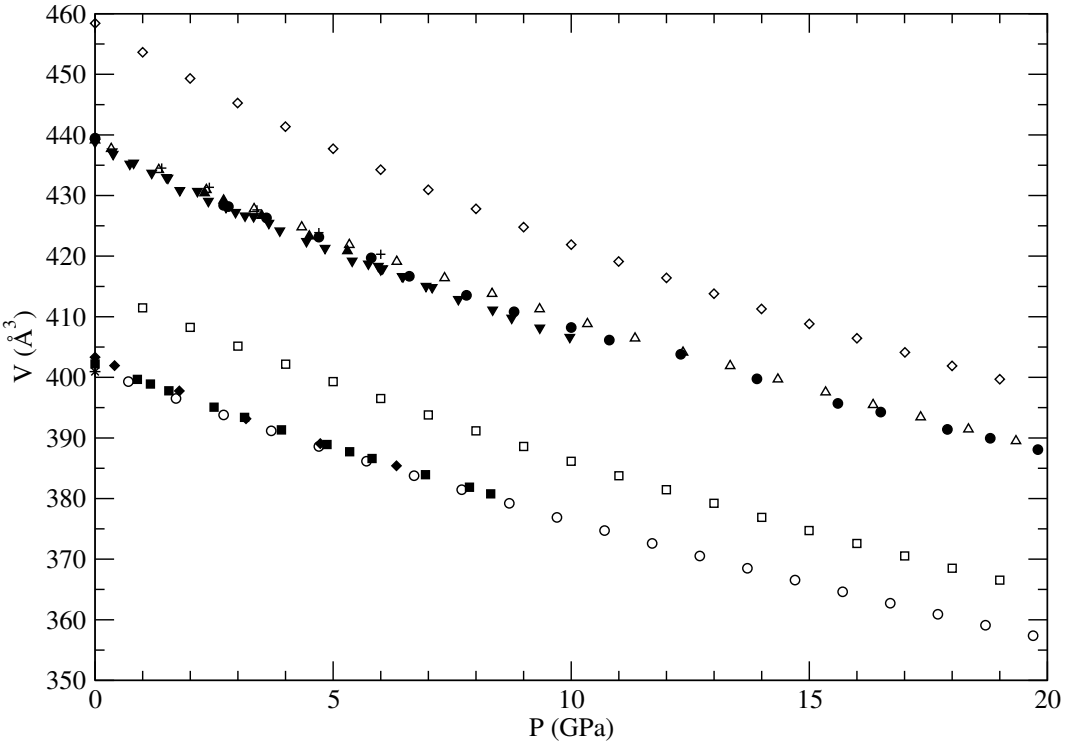

Fig. 1. Unit cell volume of jadeite and diopside as a function of pressure from these calculations (open symbols; squares: uncorrected jadeite, circles: jadeite with pressure correction, diamonds: uncorrected diopside, triangles: diopside with pressure correction) and experiments. Experimental results are shown with filled symbols: squares, diamonds and star: jadeite (Nestola et al., 2006; Zhao et al., 1997; Knight and Price, 2008, respectively), circles, upward pointing triangles, downward pointing triangles and crosses: diopside (Tribaudino et al., 2000; Levien and Prewitt, 1981; Zhang et al., 1997; McCormick et al., 1989, respectively).

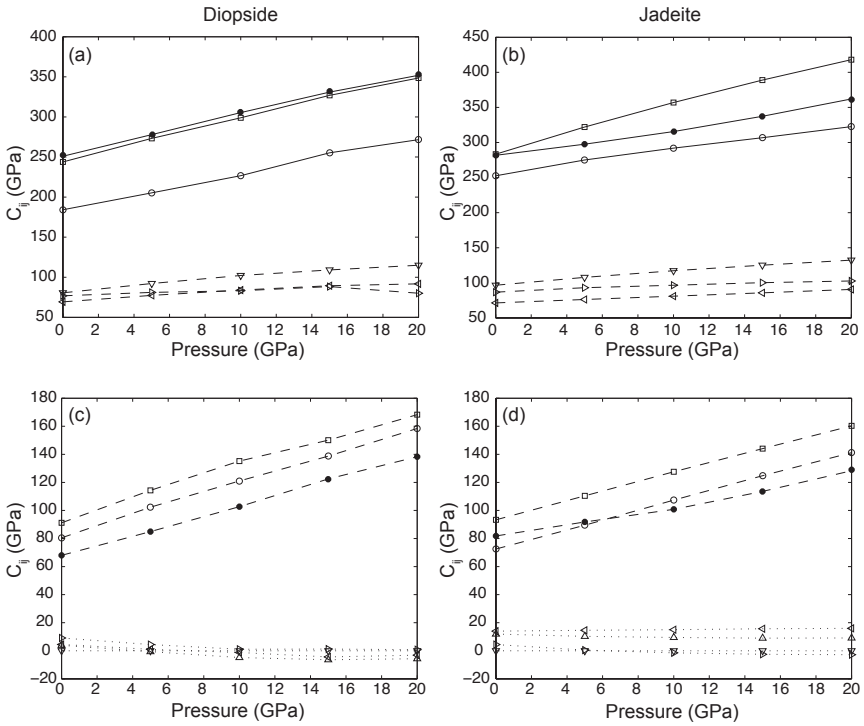

Fig. 2. Evolution of the elastic constants of diopside, (a) and (c), and jadeite, (b) and (d), as a function of pressure. Pressure is corrected for the under binding of the GGA. Parts (a) and (b) show the longitudinal (solid lines – squares: C_{11}, unfilled circles: C_{22}, filled circles: C_{33} and shear (dashed lines – right pointing triangle: C_{44}, left pointing triangle: C_{55}, downwards pointing triangle: C_{66}) constants. Parts (c) and (d) show the off diagonal constants (dashed lines – squares: C_{12}, unfilled circles: C_{13}, filled circles: C_{23}; dotted lines – right pointing triangle: C_{15}, left pointing triangle: C_{25}, downwards pointing triangle: C_{65}, upwards pointing triangle: C_{43}). Calculated errors on the elastic constants are smaller than the symbol size. Numerical values are given in the Supplementary Information.

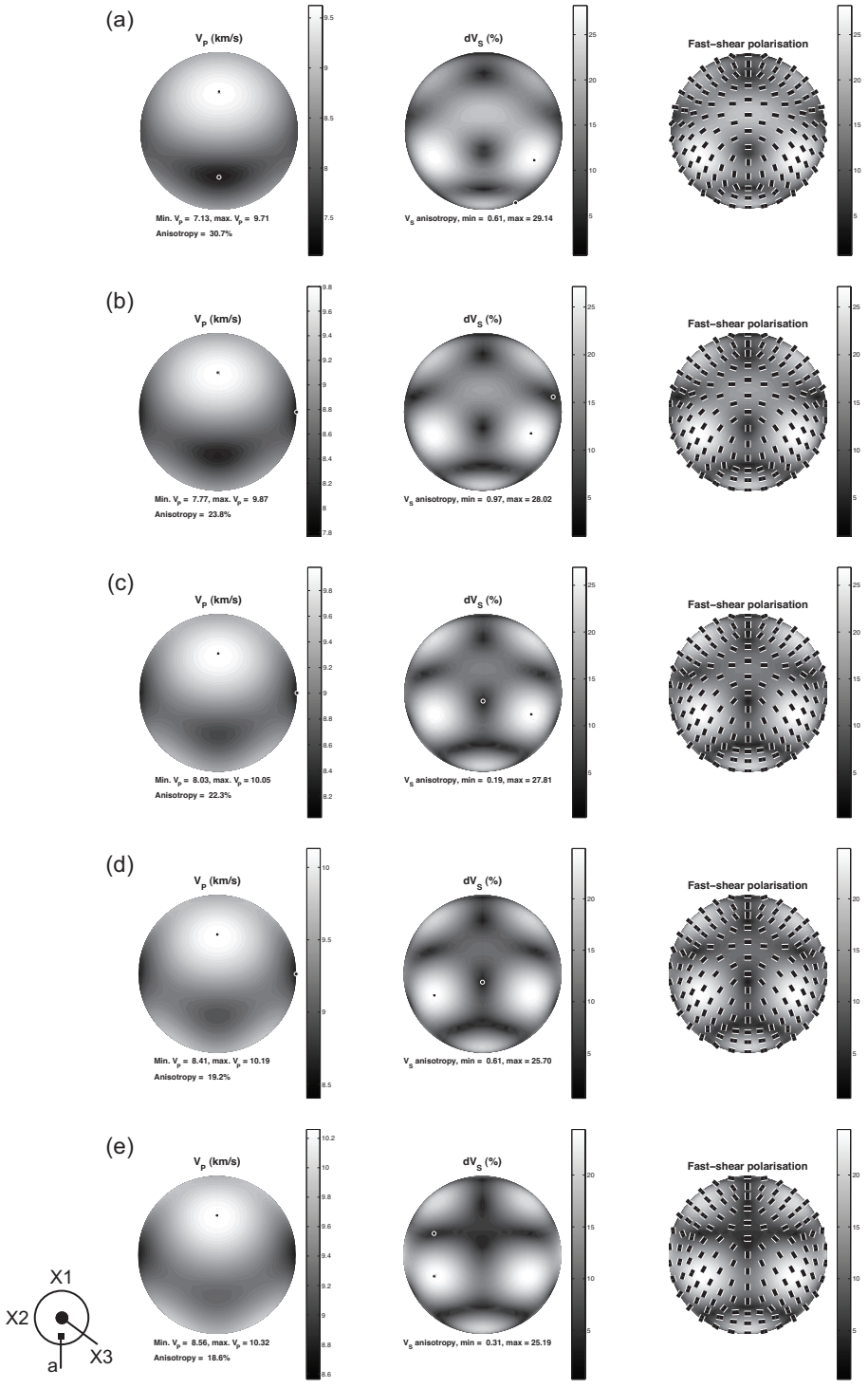

Fig. 3. Wave velocities and anisotropy in diopside at 0 GPa (a), 5 GPa (b), 10 GPa (c), 15 GPa (d) and 20 GPa (e). Upper hemisphere pole figures with cartesian axis system and approximate location of crystallographic a axis shown in the inset (b is parallel to X2 and c is parallel to X3).

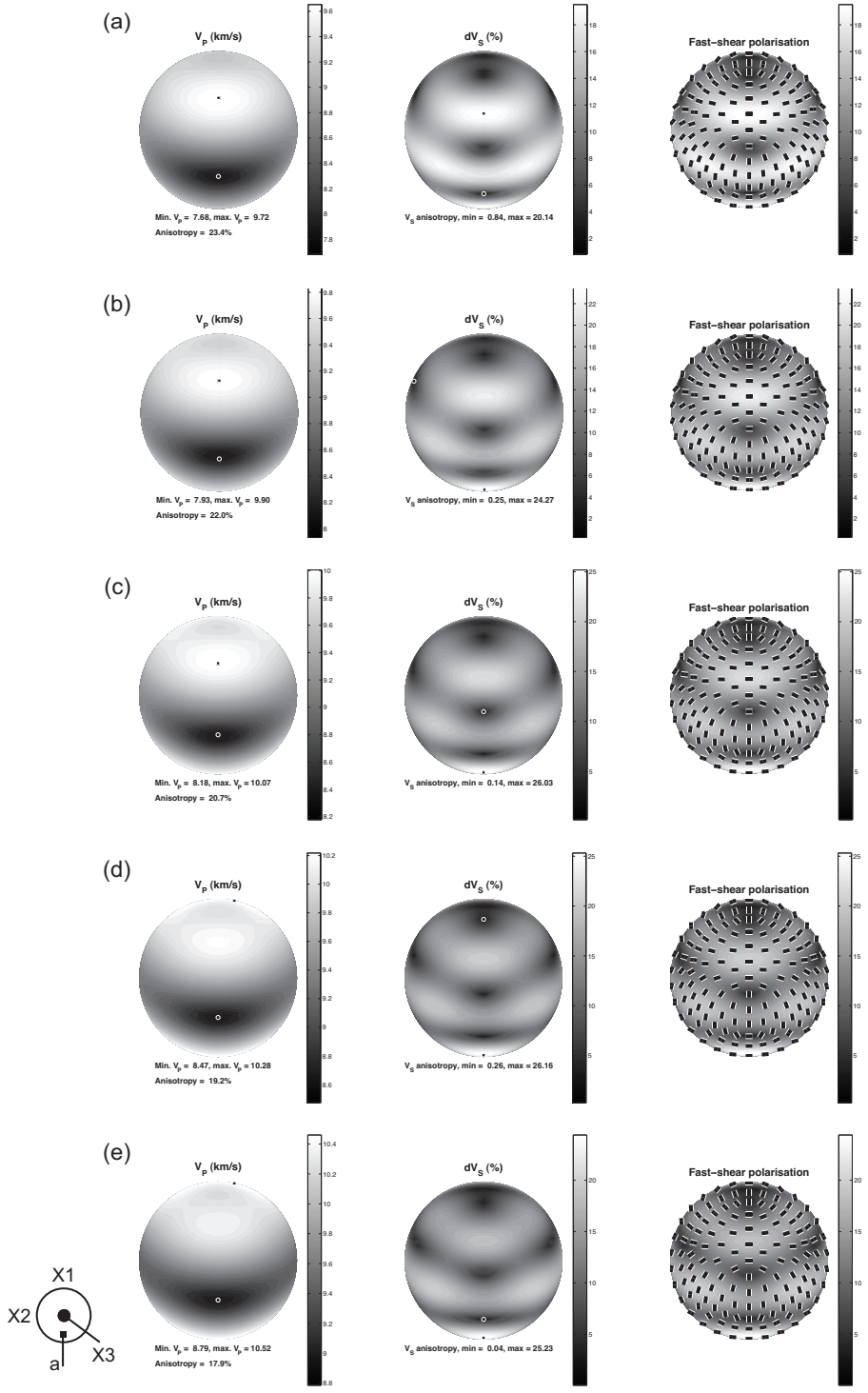

Fig. 4. Wave velocities and anisotropy in jadeite at 0 GPa (a), 5 GPa (b), 10 GPa (c), 15 GPa (d) and 20 GPa (e). Upper hemisphere pole figures with cartesian axis system and approximate location of crystallographic a axis shown in the inset (b is parallel to X2 and c is parallel to X3).